RESEARCH ARTICLE

Reversible Modulation of Plasmonic Coupling of Gold Nanoparticles Confined within Swellable Polymer Colloidal Spheres

Zuyang Ye,[a] Chen Chen,[a] Licheng Cao,[a] Zepeng Cai,[a] Christina Xu,[a] Hye-In Kim,[b] Juan Pablo Giraldo,[b] Antonios G. Kanaras,[c] Yadong Yin*[a]

[a] Z. Ye, C. Chen, L. Cao, Z. Cai, C. Xu, Prof. Dr. Y. Yin
Department of Chemistry
University of California, Riverside
Riverside, CA 92521 (USA)
E-mail: yadong.yin@ucr.edu

[b] Dr. H.-I. Kim, Prof. Dr. J. P. Giraldo
Department of Botany and Plant Sciences
University of California, Riverside
Riverside, CA 92521 (USA)

[c] Prof. Dr. A. G. Kanaras
School of Physics and Astronomy, Faculty of Engineering and Physical Sciences
University of Southampton
Southampton SO171BJ (UK)

Supporting information for this article is given via a link at the end of the document.

Abstract: Dynamic optical modulation in response to stimuli provides exciting opportunities for designing novel sensing, actuating, and authentication devices. Here, we demonstrate that the reversible swelling and deswelling of crosslinked polymer colloidal spheres in response to pH and temperature changes can be utilized to drive the assembly and disassembly of the embedded gold nanoparticles (AuNPs), inducing their plasmonic coupling and decoupling and, correspondingly, color changes. The multi-responsive colloids are created by depositing a monolayer of AuNPs on the surface of resorcinol-formaldehyde (RF) nanospheres, then overcoating them with an additional RF layer, followed by a seeded growth process to enlarge the AuNPs and reduce their interparticle separation to induce significant plasmonic coupling. This configuration facilitates dynamic modulation of plasmonic coupling through the reversible swelling/deswelling of the polymer spheres in response to pH and temperature changes. The rapid and repeatable transitions between coupled and decoupled plasmonic states of AuNPs enable reversible color switching when the polymer spheres are in colloidal form or embedded in hydrogel substrates. Furthermore, leveraging the photothermal effect and stimuli-responsive plasmonic coupling of the embedded AuNPs enables the construction of hybrid hydrogel films featuring switchable anticounterfeiting patterns, showcasing the versatility and potential of this multi-stimuli-responsive plasmonic system.

Introduction

Plasmonic nanoparticles, particularly those composed of gold and silver, have garnered immense research interest due to their unique localized surface plasmon resonance (LSPR) properties.[1-3] The ability of these nanoparticles to confine and enhance electromagnetic fields at the nanoscale, coupled with their tunable optical properties, has enabled a diverse array of applications spanning catalysis,[4-6] biotechnologies,[7-9] and optical devices.[10-12] While the LSPR properties of plasmonic nanoparticles have been conventionally modulated by tailoring their physical parameters, such as size, shape, and composition,[13-17] recent research efforts have increasingly focused on achieving dynamic regulation of these properties.[18-20] For instance, integrating plasmonic nanoparticles with stimuli-responsive materials enables the modulation of the interparticle spacing or the local dielectric environment around the nanoparticles in response to external stimuli, such as pH,[21, 22] temperature,[23, 24] light,[25, 26] and magnetic fields.[27, 28] Leveraging these stimuli-responsive mechanisms makes it possible to dynamically and reversibly tune the LSPR properties of plasmonic nanoparticles, thereby expanding their functional capabilities and potential applications.

Despite considerable progress in the dynamic tuning of LSPR and its successful application in fields such as optical anticounterfeiting technologies, most current systems are limited to single-stimulus responses. The ability to combine multiple stimuli-responsive mechanisms is highly desirable, as it facilitates multilevel and multimodal anticounterfeiting, making the encoded information more difficult to replicate and thus enhancing security levels.[29-32] However, research into multi-stimuli-responsive plasmonic systems has been relatively scarce and largely limited to solution phases, mainly due to the lack of effective strategies for controlling the spatial arrangement of plasmonic particles in solid matrices without causing irreversible damage under external stimuli.

In this work, we introduce a multi-responsive plasmonic system capable of reversible and dynamic modulation of its plasmonic coupling states. By confining a monolayer of plasmonic

nanoparticles within swellable polymer spheres, we show that the hybrid nanostructures exhibit multiple coupling states due to the multi-responsive swelling behavior of the polymer. Specifically, we have developed hybrid nanostructures comprised of a gold nanoparticle (AuNP) monolayer encapsulated between resorcinol-formaldehyde (RF) cores and shells. The plasmonic coupling is enabled by enlarging the AuNPs and reducing interparticle separation through a space-confined seeded growth method. The swelling of RF can be triggered by base treatment, which deprotonates phenol groups and may disrupt methylene bridge bonds within the RF matrix, increasing solvent permeability and facilitating polymer expansion. Conversely, sequential treatment with acid and heat can reverse this process, inducing the deswelling of RF. This dynamic swelling and deswelling behavior effectively regulates the interparticle spacing of AuNPs, enabling rapid and repeatable decoupling and recoupling of their localized surface plasmons. Notably, the one-step decoupling through base treatment and two-step coupling through sequential acid and heat treatment enable switchable color transitions among ternary states in both solution and solid films. By harnessing the photothermal effect and stimuli-responsive reversible coupling of this plasmonic system, dynamic anticounterfeiting patterns can be created by laser irradiation. Further, to illustrate the versatility and adaptability of this multi-responsive plasmonic coupling system, we have demonstrated information encryption patterns capable of displaying varied information in response to different stimuli. These patterns feature reversibility and reusability, highlighting the broad application potential of the novel multi-responsive plasmonic system.

Results and Discussion

The synthesis of AuNPs with reversible plasmonic coupling within RF matrices is illustrated in Figure 1a. RF nanospheres were produced via a modified Stöber method and subsequently functionalized with (3-aminopropyl)triethoxysilane (APTES) to introduce amine groups onto the RF surface for the immobilization of gold seeds. An additional RF layer was then coated onto the gold-seed decorated RF spheres, which offered several key advantages: (1) its physical confinement, together with the flexible and porous nature of the polymer, allows for controlling the seeded growth of AuNPs; (2) it serves as an intrinsic reducing agent for the gold precursor ($AuCl_4^-$), eliminating the need for additional reducing agents and preventing undesired self-nucleation of AuNPs; (3) it provides steric hindrance to mitigate nanoparticle aggregation during subsequent manipulations and applications. The transmission electron microscopy (TEM) image in Figure 1b depicted typical RF@Au(s)@RF hybrid nanostructures before the seeded growth process, where a monolayer of tiny gold seeds with an average size of 3 nm was embedded between RF cores and shells. The subsequent growth of the gold seeds increased their sizes and effectively reduced their interparticle distance, as evidenced in Figure 1c**,** which illustrates a layer of densely packed AuNPs with an average size of 14 nm around each RF core (RF@Au@RF). Consistently, the color of the colloidal dispersion noticeably deepened as the seed growth progressed, indicating the gradual establishment of plasmonic coupling among AuNPs. The UV-Vis-NIR extinction spectra shown in Figure 1d provided further evidence of plasmonic coupling. Initially, a plasmonic peak emerged at ~550 nm, corresponding to the grown AuNPs inside RF. As more $HAuCl_4$ was added, this peak gradually red-shifted to ~700 nm, along with the peak broadening. These spectral changes are consistent with the random coupling among the densely packed plasmonic nanoparticles embedded within the RF matrices.[33, 34]

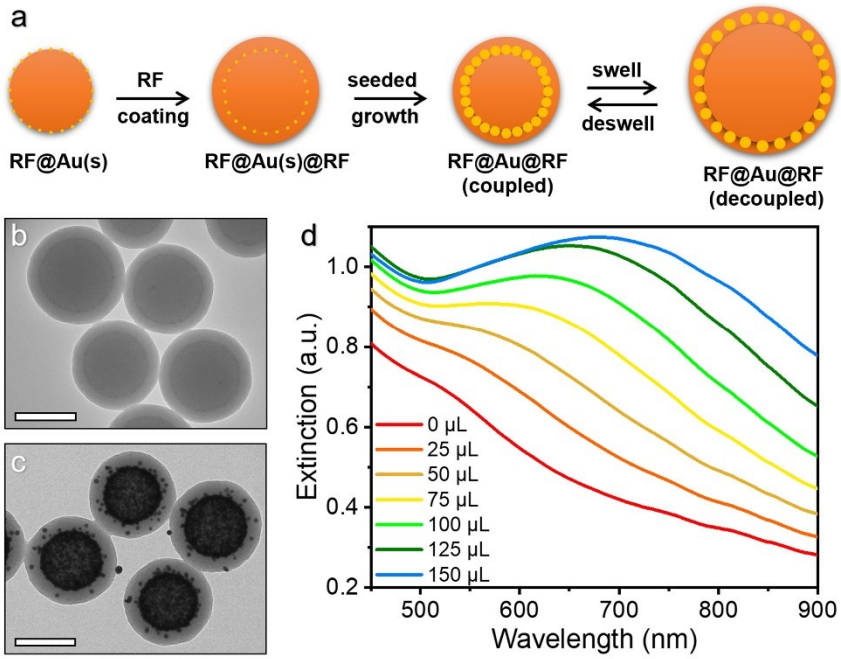

Figure 1. Design of the multi-stimuli-responsive plasmonic coupling system with a monolayer of AuNPs confined in RF spheres. a) Schematic illustration of the preparation process. b, c) TEM images of typical RF@Au@RF spheres (b) before and (c) after the space-confined seeded growth process. The scale bars are 200 nm. d) Extinction spectra showing the evolution of plasmonic peaks during the seeded growth of AuNPs with varying quantities of $HAuCl_4$.

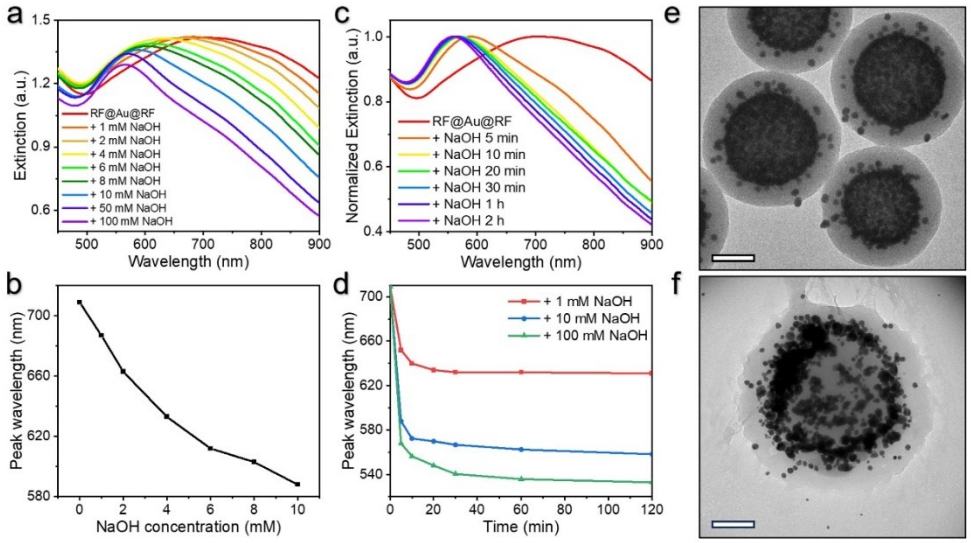

Figure 2. Decoupling of surface plasmons in AuNPs via base-induced swelling of RF polymer. a, c) Extinction spectra showing the shift of plasmonic peaks with the treatment of different concentrations of NaOH for 5 min (a) and 10 mM of NaOH for different periods (c). b, d) Changes in the plasmonic peak wavelength as a function of NaOH concentrations after 5 min treatment (b) and NaOH treatment time with different NaOH concentrations (d). e, f) TEM images of typical RF@Au@RF samples after treatment with (e) 10 mM and (f) 100 mM of NaOH for 2 h. The scale bars are 100 nm.

We further investigated the modulation of plasmonic coupling of the hybrid nanostructures in response to chemical stimuli. Figure 2 elucidates the decoupling of surface plasmons within the RF@Au@RF nanostructures upon exposure to an alkaline environment. Upon adding NaOH, the colloidal dispersion of the RF@Au@RF nanostructures exhibited a pronounced blue shift and gradual narrowing in their plasmonic peak (Figure 2a and b). This spectral shift was dependent on the NaOH concentration, where a substantial decoupling was attained by treating the aqueous RF@Au@RF dispersion with 100 mM of NaOH for 5 min, transitioning the plasmonic peak from ~700 nm to ~570 nm. Kinetic studies revealed a rapid disassembly process, with a marked shift occurring within the initial 5 min of NaOH exposure and reaching equilibrium within 1 hour (Figure 2c and d). Such swift reaction enabled rapid decoupling of AuNPs, reverting to a simple resonance mode of isolated AuNPs.

Further morphological insights were gained through TEM imaging. As shown in Figure 2e, treatment with a relatively low concentration (<10 mM) of NaOH led to negligible morphological changes in the RF@Au@RF sample, although it was sufficient to induce plasmonic decoupling. In contrast, samples treated with a significantly higher concentration (100 mM) of NaOH showed significant swelling of the RF structure, along with a more pronounced spatial separation of the AuNPs (Figure 2f). These results suggested that NaOH treatment induced swelling within the RF matrix, causing the displacement and increased interparticle distances of the embedded AuNPs, ultimately leading to the observed decoupling of surface plasmons. However, it is important to note that the TEM measurements were performed under dry conditions, potentially underestimating the actual swelling behavior of the RF matrix and the spatial arrangement of AuNPs in the aqueous environment.

More comprehensive analyses were conducted to gain deeper insights into the mechanism of plasmonic peak shifts in RF@Au@RF samples. Dynamic light scattering (DLS) analysis confirmed the base-mediated swelling of the RF matrix (Figure 3a). The average hydrodynamic diameters of the RF@Au@RF samples exhibited a substantial increase from 500 nm to 531 nm, 630 nm, and 730 nm, upon treatment with NaOH at concentrations of 1 mM, 10 mM, and 100 mM of NaOH, respectively. This trend demonstrated the pronounced swelling of RF, which intensifies with increasing base concentration. COMSOL simulations were performed to correlate the swelling of the RF matrix and the decoupling of RF@Au@RF nanostructures (Figure 3b, S2). The model consisted of an RF nanosphere with five peripherally attached AuNPs, exhibiting a plasmonic coupling peak at 780 nm. To simulate the swelling effect, the diameter of the RF nanosphere was progressively increased while maintaining the relative positions of the attached AuNPs. As the RF swelled, the interparticle distances between AuNPs increased correspondingly. As shown in Figure 3b and c**,** a modest swelling of 0.5% could induce a discernible blue shift in the coupling peak from 780 nm to 730 nm. Further swelling led to additional blue shifts of the coupling peaks, which ultimately shifted the peak to 580 nm at a swelling of 10%. These results revealed that the base-induced swelling of RF facilitated the spatial separation of the embedded AuNPs, resulting in plasmon decoupling and consequent blue shift in plasmonic peaks. Additionally, swelling of the RF matrix decreases its refractive index, leading to a blue shift of in the coupling peaks. However, as shown in Figure S3, these changes in refractive index contribute minimally to the peak shifts when compared to the effects of decoupling, suggesting that the dominant mechanism influencing the observed color changes is plasmonic decoupling, rather than refractive index variations.

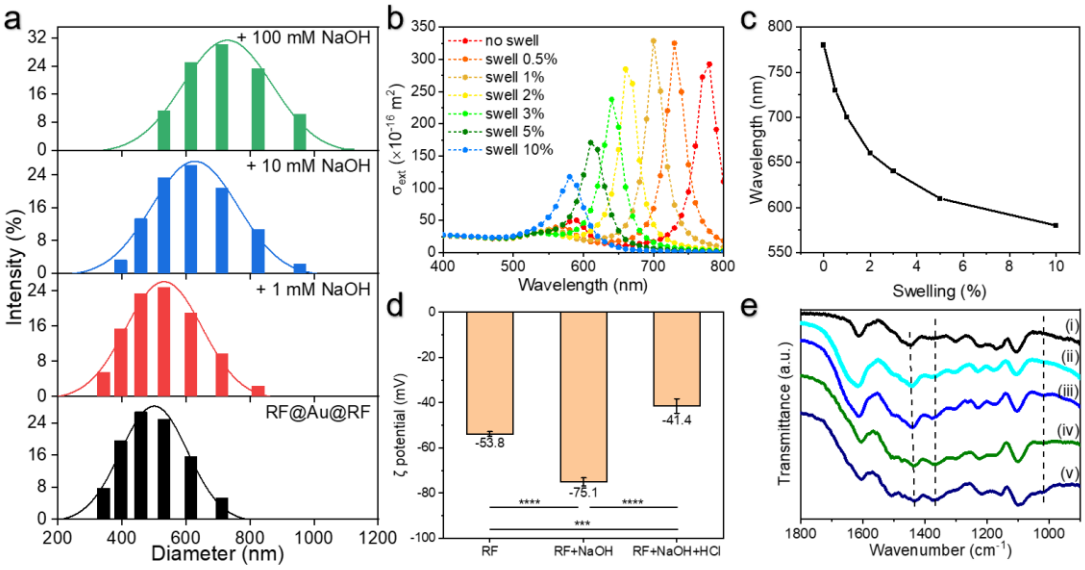

Figure 3. Mechanism study of swelling-induced decoupling of AuNP confined in RF polymer. a) DLS size distributions of RF@Au@RF nanoparticles treated with different concentrations of NaOH. b) Simulated extinction profile of Au nanoparticle chains attached to the polymer of varying swelling ratios with the incident light polarized along the y-axis. c) Changes in the peak wavelength of plasmonic coupling of Au nanoparticle chains as a function of swelling ratio. d) The zeta potential of RF nanospheres with different treating conditions. The error bars represent the standard deviation of three independent measurements of the same sample. Means were compared by one-way ANOVA followed by post hoc comparison using the Tukey test. **** $p < 0.0001$. *** $p < 0.005$. e) FTIR spectra of RF nanospheres (i) as-synthesized and (ii-v) treated with 100 mM of NaOH for (ii) 1 h, (iii) 2 h, (iv) 4 h, and (v) 8 h.

We further investigated the reasons for the swelling behavior of the RF matrix in alkaline conditions. As shown in Figure 3d, the zeta potential of RF nanoparticles shifted from -53.8 mV to -75.1 mV after being treated with 0.1 M NaOH, indicating an increased surface negative charge due to the deprotonation of phenol groups present in the RF molecules. This enhanced surface charge increases the electrostatic repulsion among RF backbones, facilitating the penetration of water molecules into the RF matrix and consequently inducing swelling. Notably, this deprotonation process was reversible, as indicated by the restoration of the zeta potential upon HCl treatment. The deprotonation process may also triggered the benzenoid-to-quinoid transition of RF, as revealed by the appearance of a new shoulder peak at ~1645 cm^{-1} in the Fourier transform infrared (FTIR) spectra, corresponding to the C=O stretching vibration in the quinoid structure (Figure 3e).[35] The characteristic vibrational bands were assigned and listed in Table S1. After NaOH treatment, the intensity of the band at ~1446 cm^{-1} decreased, suggesting a reduced amount of methylene bridges within the RF matrix.[35, 36] In contrast, the intensification of bands at 1370 cm^{-1} and 1014 cm^{-1} indicated an increased amount of hydroxymethyl groups.[37] These spectral changes indicated the cleavage of methylene bridges and the formation of hydroxymethyl groups, decreasing the crosslinking degree and consequently enhancing the permeability of the RF matrix.[38] Therefore, the base treatment may modulate the RF matrix through a dual mechanism. Firstly, it deprotonates the phenolic hydroxyl groups, creating negative charges that augment electrostatic repulsion among RF backbones and facilitate the penetration of solvent molecules. Secondly, strong bases may cleave methylene bridge bonds, reducing the crosslinking degree of RF and, therefore, enhancing its permeability. Collectively, these two functions synergistically contribute to the pronounced swelling of the RF matrix observed under alkaline conditions.

The above mechanism enabled reversible swelling/deswelling of the RF matrix. The base-induced deprotonation process could be reversed by introducing an acid. Upon adding HCl to the aqueous dispersion of the deprotonated RF@Au@RF particles, the RF matrix underwent reprotonation, triggering the reassembly of AuNPs into a coupled state and redshifting the plasmonic peak (Figure 4a). Conversely, introducing NaOH into the same dispersion gradually reversed the coupling process (Figure 4b). This reversible modulation was visually evidenced by the color transition of the dispersion between purple and blue, corresponding to the decoupled and coupled state of AuNPs, respectively, which could be cycled through multiple times (Figure 4c and d). Additionally, to counteract the reduced crosslinking of the RF matrix caused by the base-induced bond cleavage, the sample was subjected to condensation at elevated temperatures to increase the crosslinking degree of RF.[39] The condensation occurs between hydroxymethyl groups, forming methylene (-CH_2-) and ether (-O-) bridges connecting phenol rings.[40] As a result, after heating at 80 ℃ for 30 min, the plasmonic coupling peak of RF@Au@RF further red-shifted, altering the color of the dispersion to green (Figure 4d and e). Therefore, complete recovery of the coupled state and its corresponding plasmonic peak was achieved through a sequential treatment of acid and heat, as shown in Figure S4. Nonetheless, it is worth noting that exposure of samples to high concentrations of NaOH (e.g., 100 mM) for extended periods (beyond 2 hours) could cause irreversible swelling of the RF matrix due to extensive etching and degradation of the polymer structure. This irreversible swelling

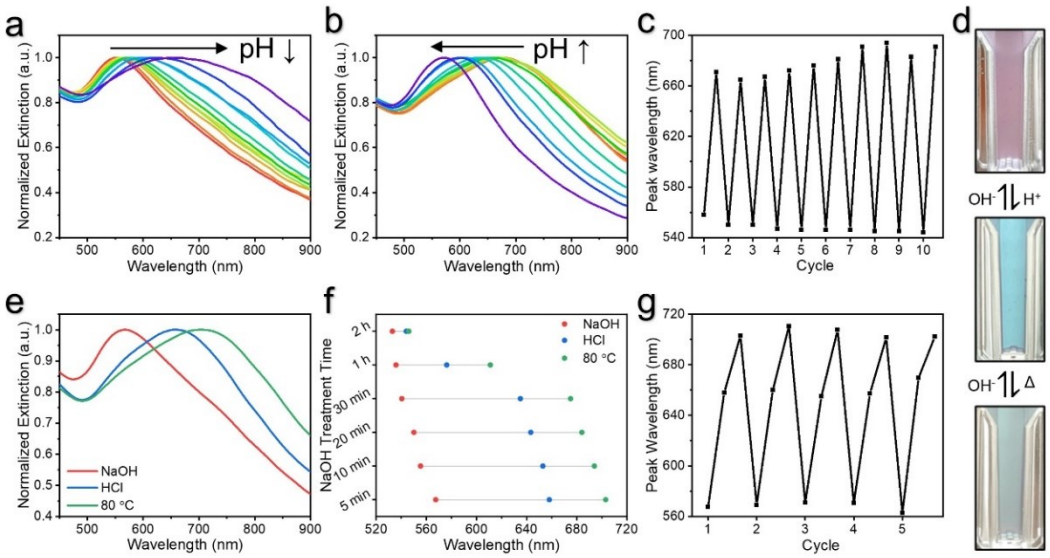

Figure 4. The pH-responsive reversible tuning of plasmonic coupling of AuNPs. a) Extinction spectra of a typical NaOH-treated RF@Au@RF dispersion when pH decreased from 12 to 2. b) Extinction spectra of a typical HCl-treated RF@Au@RF dispersion when pH increased from 2 to 12. pH difference is 1 between neighboring spectra. c) Repeated switching of plasmonic peak positions between pH 12 and 2 for ten cycles. d) digital images showing the transmitted colors of RF@Au@RF dispersion switching between fully decoupled (top), partially coupled (middle) and fully coupled (bottom) states in response to pH changes and thermal treatment. e) Extinction spectra of RF@Au@RF dispersion treated with 100 mM of NaOH for 5 min (red curve), followed by protonation with 100 mM of HCl for 5 min (blue curve), and condensation under 80 ℃ for 30 min (green curve). f) The shift of plasmonic peak positions of samples with various NaOH (100 mM) treatment periods, followed by HCl treatment and 80 ℃ condensation. g) Repeated switching of plasmonic peak positions between pH 12, pH 2, and 80 ℃ condensation for five cycles.

prevented the reassembly of embedded AuNPs, making their plasmonic peaks unrecoverable, as demonstrated in Figure 4f. Treatment with NaOH of moderate concentration (< 10 mM) made it possible to repeat the coupling and decoupling processes over 5 cycles (Figure 4g).

In this polymer-confined system, the plasmonic decoupling induced by NaOH treatment is robust against variations in ionic strength, maintaining the decoupled state even in high ionic environments, as evidenced by the unchanged coupling peak (Figure S5). Additionally, the reversible process was independent of ionic strength and the hybrid particles could be coupled again after acid treatment, demonstrating the stability of this system in high ionic environments.

Moreover, the RF@Au@RF hybrid nanostructures could be incorporated into polymer films for versatile applications, for example, by UV-curing mixtures of RF@Au@RF spheres and a polyacrylamide pregel solution. These hydrogel films exhibited reversible color changes upon exposure to NaOH, HCl, and heat, similar to the behavior observed in colloidal dispersions (Figure 5a). It is worth highlighting that the heat stimulus may be generated internally from the hybrid nanostructure, for example, through photothermal conversion of the embedded AuNPs. As the photothermal effect is localized to AuNPs, it enables quick and region-selective heating of the film. As shown in Figure 5b and S6, under 532-nm laser illumination, the temperature of the film rapidly increases, causing the RF matrix to condense and facilitating the plasmonic coupling of the AuNPs.

The photothermal effect and the responsive plasmonic coupling of the hybrid film could be integrated to create dynamic anticounterfeiting patterns. As shown in Figure 5c, the number "2024" was written onto the base-treated hybrid film using a 532 nm laser. Immersing the film in an HCl solution resulted in the blurring of the embedded digits due to the plasmonic coupling among particles in both the numeral region and background, uniformly presenting a blue color. Reversibly, the film revealed digits "2024" again upon immersion in NaOH solution, showcasing the reversible nature of this pattern display by simply changing the pH of the film. Moreover, the acid-treated film could also be heated under laser irradiation due to the broadband absorption of AuNPs. As shown in Figure 5d, a triangle pattern was created onto the film with a photomask. Under alkaline conditions, the pattern remained blue while the surrounding area turned purple. This color transition could be reversibly switched by acid and base treatment. Additionally, heating allowed for the complete erasure of patterns, enabling the resetting of the film for creating new switchable patterns (Figure 5d and S7). Further, an anticounterfeiting film capable of selectively displaying different information under various conditions was fabricated (Figure 5e). Initially, the letters "I" and "U" were written using a laser on the base-treated film. Following acid treatment and additional laser writing, a heart-shaped pattern appeared. Under alkaline conditions, the film showed both letters and the heart shape. In contrast, under acidic conditions, only the heart shape remained visible, with the letters disappearing. Subsequent heating erased all patterns, demonstrating the reusability of the film for new information encoding. While the reversible patterns in our system can be erased by heating, they remain stable under ambient conditions. For applications where dehydration needs to be limited for long-term storage, the films could be sealed in

containers under a humid atmosphere, which could maintain their functionalities for several months.[31] This system

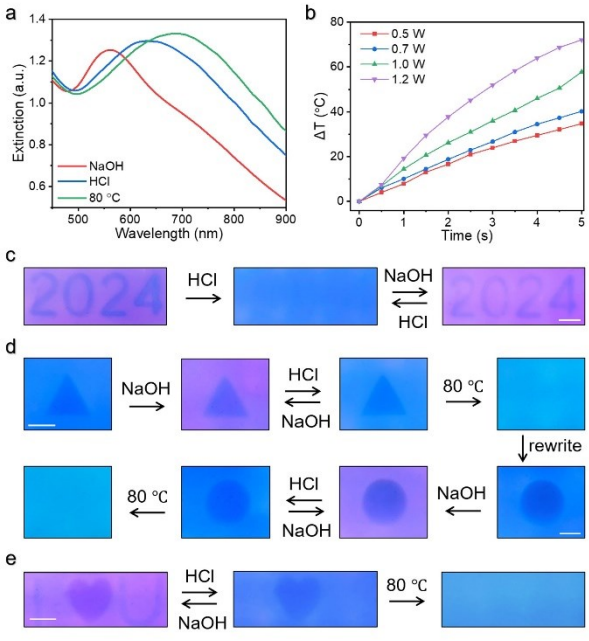

Figure 5. RF@Au@RF hybrid nanostructures for anticounterfeiting applications. a) Extinction spectra of RF@Au@RF/gel film treated with NaOH (red curve), HCl (blue curve), and heat (green curve). b) Temperature increases of hybrid films after irradiation with laser of different powers. c) Digital images of switchable patterns showing the numbers "2024" created on RF@Au@RF/gel film after 532-nm laser illumination and their diverse color states under basic and acidic conditions. d) Digital images of rewritable patterns showing diverse colors under basic and acidic conditions and could be erased by heating. e) Digital images of the anticounterfeiting film showing different information under different conditions. The scale bars in (c-e) are 5 mm.

provided an innovative approach to achieving highly customizable and dynamically changeable anticounterfeiting patterns through simple photothermal control and multi-stimulus response. Developing such an erasable anti-counterfeiting platform may be beneficial to specific applications that require self-erasing of the security information. The reusability may also help reduce materials costs and decrease environmental impact,[30, 41, 42] opening new avenues for advanced anticounterfeiting applications.

Conclusion

We have developed a novel multi-stimuli-responsive plasmonic coupling system utilizing monolayers of AuNPs confined within swellable polymer spheres, enabling reversible and dynamic modulation of plasmonic properties through pH changes and thermal treatment. The base-induced swelling of the RF matrix facilitates the decoupling of AuNPs, while the subsequent acid treatment and heating induce deswelling, leading to the recoupling of the nanoparticles. The stimuli-responsive behavior and the photothermal effect of the hybrid particles enable the generation of color patterns for anticounterfeiting applications, which showcase reversible and rewritable patterns and selective information display. Introducing swellable polymer spheres with multi-stimulus responses to control plasmonic coupling offers new directions for developing adaptive optical materials and advanced anticounterfeiting technologies.

Acknowledgements

The authors are grateful for the financial support from the U.S. National Science Foundation (CHE- 2203972).

Keywords: nanoparticles • plasmonic coupling • reversible modulation • stimuli-responsive • swelling

[1] J. Chen, Z. Ye, F. Yang, Y. Yin, *Small Sci.* **2021**, *1*, 2000055.
[2] J. Zheng, X. Cheng, H. Zhang, X. Bai, R. Ai, L. Shao, J. Wang, *Chem. Rev.* **2021**, *121*, 13342-13453.
[3] Y. Hang, A. Wang, N. Wu, *Chem. Soc. Rev.* **2024**, *53*, 2932-2971.
[4] S. Luo, X. Ren, H. Lin, H. Song, J. Ye, *Chem. Sci.* **2021**, *12*, 5701-5719.
[5] A. G. M. da Silva, T. S. Rodrigues, J. Wang, P. H. C. Camargo, *Chem. Commun.* **2022**, *58*, 2055-2074.
[6] Y. Dong, C. Hu, H. Xiong, R. Long, Y. Xiong, *ACS Catal.* **2023**, *13*, 6730-6743.
[7] Z. Li, W. Poon, Z. Ye, F. Qi, B. H. Park, Y. Yin, *ACS Nano* **2022**, *16*, 12738-12746.
[8] Z. Li, Z. Meng, F. Tian, Z. Ye, X. Zhou, X. Zhong, Q. Chen, M. Yang, Z. Liu, Y. Yin, *Nano Lett.* **2022**, *22*, 5158-5166.
[9] L. Zhan, S. Z. Guo, J. Kangas, Q. Shao, M. Shiao, K. Khosla, W. C. Low, M. C. McAlpine, J. Bischof, *Adv. Sci.* **2021**, *8*, 2004605.
[10] J. Feng, F. Yang, X. Wang, F. Lyu, Z. Li, Y. Yin, *Adv. Mater.* **2019**, *31*, e1900789.
[11] C. Wu, Q. Fan, Z. Li, Z. Ye, Y. Yin, *Mater. Horiz.* **2024**, *11*, 680-687.
[12] Z. Li, J. Zhang, J. Jin, F. Yang, R. Aleisa, Y. Yin, *J. Am. Chem. Soc.* **2021**, *143*, 15791-15799.
[13] J. Chen, J. Feng, F. Yang, R. Aleisa, Q. Zhang, Y. Yin, *Angew. Chem. Int. Ed.* **2019**, *131*, 9376-9382.
[14] J. Chen, Y. Bai, J. Feng, F. Yang, P. Xu, Z. Wang, Q. Zhang, Y. Yin, *Angew. Chem. Int. Ed.* **2021**, *133*, 4163-4170.
[15] J. Feng, D. Xu, F. Yang, J. Chen, C. Wu, Y. Yin, *Angew. Chem. Int. Ed.* **2021**, *60*, 16958-16964.
[16] F. Yang, J. Feng, J. Chen, Z. Ye, J. Chen, D. K. Hensley, Y. Yin, *Nano Res.* **2022**, *16*, 5873-5879.
[17] M. Sayed, J. Yu, G. Liu, M. Jaroniec, *Chem. Rev.* **2022**, *122*, 10484-10537.
[18] J. Cheng, E. H. Hill, Y. Zheng, T. He, Y. Liu, *Mater. Chem. Front.* **2018**, *2*, 662-678.
[19] Z. Li, W. Wang, Y. Yin, *Trends Chem.* **2020**, *2*, 593-608.
[20] F. Neubrech, X. Duan, N. Liu, *Sci. Adv.* **2020**, *6*, eabc2709.
[21] J.-W. Jeon, J. Zhou, J. A. Geldmeier, J. F. Ponder, M. A. Mahmoud, M. El-Sayed, J. R. Reynolds, V. V. Tsukruk, *Chem. Mater.* **2016**, *28*, 7551-7563.
[22] L. Liu, Z. Gao, B. Jiang, Y. Bai, W. Wang, Y. Yin, *Nano Lett.* **2018**, *18*, 5312-5318.
[23] M. Nguyen, N. Felidj, C. Mangeney, *Chem. Mater.* **2016**, *28*, 3564-3577.
[24] T. Ding, J. J. Baumberg, *Nanoscale Adv.* **2020**, *2*, 1410-1416.
[25] X. Lu, Y. Huang, B. Liu, L. Zhang, L. Song, J. Zhang, A. Zhang, T. Chen, *Chem. Mater.* **2018**, *30*, 1989-1997.

[26] A. Jedrych, M. Pawlak, E. Gorecka, W. Lewandowski, M. M. Wojcik, *ACS Nano* **2023**, *17*, 5548-5560.
[27] F. Qi, L. Li, Z. Li, L. Qiu, Z. Meng, Y. Yin, *ACS Nano* **2023**, *17*, 1427-1436.
[28] J. N. Li, G. Li, X. G. Lu, S. C. Wang, M. Y. Leng, S. Yang, J. G. Guan, Y. Long, *Adv. Funct. Mater.* **2024**, *34*, 2308293.
[29] X. Zhou, L. Ning, J. Qiao, Y. Zhao, P. Xiong, Z. Xia, *Nat. Commun.* **2022**, *13*, 7589.
[30] H. Q. Wang, Y. Tang, Z. Y. Huang, F. Z. Wang, P. F. Qiu, X. Zhang, C. H. Li, Q. Li, *Angew. Chem. Int. Ed.* **2023**, *62*, e202313728.
[31] Z. Ye, Z. Li, J. Feng, C. Wu, Q. Fan, C. Chen, J. Chen, Y. Yin, *ACS Nano* **2023**, *17*, 18517-18524.
[32] Y. Shen, X. Le, Y. Wu, T. Chen, *Chem. Soc. Rev.* **2024**, *53*, 606-623.
[33] J. Chen, M. Gong, Y. Fan, J. Feng, L. Han, H. L. Xin, M. Cao, Q. Zhang, D. Zhang, D. Lei, Y. Yin, *ACS Nano* **2022**, *16*, 910-920.
[34] M. Kim, K. P. Kubelick, A. M. Yu, D. Vanderlaan, A. Jhunjhunwala, R. J. Nikolai, M. Cadena, J. Kim, S. Y. Emelianov, *Adv. Funct. Mater.* **2024**, 2313963.
[35] Y. Shiraishi, T. Takii, T. Hagi, S. Mori, Y. Kofuji, Y. Kitagawa, S. Tanaka, S. Ichikawa, T. Hirai, *Nat. Mater.* **2019**, *18*, 985-993.
[36] M. Zhang, H. Song, Y. Yang, X. Huang, Y. Liu, C. Liu, C. Yu, *Angew. Chem. Int. Ed.* **2018**, *57*, 654-658.
[37] L. Pilato, *Phenolic Resins: A Century of Progress*, Springer Berlin Heidelberg, Berlin, **2010**.
[38] L. M. Pratt, R. Szostak, I. M. Khan, J. Bibler, *J. Macromol. Sci. Pure Appl. Chem.* **1997**, *34*, 281-289.
[39] Z.-L. Yu, Y.-C. Gao, B. Qin, Z.-Y. Ma, S.-H. Yu, *Acc. Mater. Res.* **2024**, *5*, 146-159.
[40] S. Liu, Z. Ye, Y. Yin, *Langmuir* **2024**, *40*, 8760-8770.
[41] X. Le, H. Shang, H. Yan, J. Zhang, W. Lu, M. Liu, L. Wang, G. Lu, Q. Xue, T. Chen, *Angew. Chem. Int. Ed.* **2021**, *60*, 3640-3646.
[42] R. Zhang, Y. Chen, Y. Liu, *Angew. Chem. Int. Ed.* **2023**, *62*, e202315749.

Entry for the Table of Contents

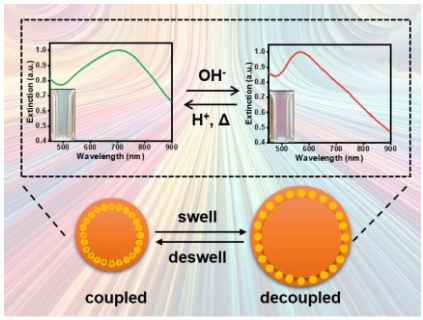

Dynamic modulation of plasmonic coupling is achieved using gold nanoparticles embedded in crosslinked polymer colloidal spheres. The swelling and deswelling of these polymer spheres in response to pH and temperature changes enable the assembly and disassembly of the gold nanoparticles, altering their plasmonic coupling and allowing reversible color switching.